

A Synthetic Nervous System for on and Off Motion Detection Inspired by the *Drosophila melanogaster* Optic Lobe

William R. P. Nourse^{1(⊠)}, Nicholas S. Szczecinski², and Roger D. Quinn³

- Department of Electrical, Computer, and Systems Engineering, Case Western Reserve University, Cleveland, OH 44106, USA nourse@case.edu
- 2 Department of Mechanical and Aerospace Engineering, West Virginia University, Morgantown, WV 26506, USA
 - ³ Department of Mechanical and Aerospace Engineering, Case Western Reserve University, Cleveland, OH 44106, USA

Abstract. In this work, we design and simulate a synthetic nervous system which is capable of computing optic flow throughout a visual field, inspired by recent advances in the neural anatomy of *Drosophila melanogaster* found through connectomics. We present methods for tuning the network for desired stimuli, and benchmark its temporal properties and capability for directional selectivity. This network acts as a stepping point towards visual locomotion control in a hexapod robot inspired by the anatomy of *Drosophila*.

Keywords: Motion Vision · Optic Flow · Synthetic Nervous System

1 Introduction

A continuing goal in the robotics community is to develop robots with the dynamic capabilities and resilience of animals. A particular focus is on adding the influence of visual information to improve the adaptability of robotic systems [4,37]. A promising approach is to design robotic controllers using neuromorphic networks of neurons with biologically inspired dynamics [3], also known as synthetic nervous systems (SNS) [13,18,31].

Much is known about the circuitry within the *Drosophila melanogaster* optic lobe, making it a convenient inspiration for robotic vision systems. For visual motion processing in particular, the *Drosophila* nervous system contains many of the same logical elements as that of mammals and vertebrates [8], but does so with three orders of magnitude fewer neurons in the visual system [6,22]. An

This work was funded by National Science Foundation (NSF) RI 1704436, as well as by NSF DBI 2015317 as part of the NSF/CIHR/DFG/FRQ/UKRI-MRC Next Generation Networks for Neuroscience Program.

[©] The Author(s), under exclusive license to Springer Nature Switzerland AG 2023 F. Meder et al. (Eds.): Living Machines 2023, LNAI 14157, pp. 364–380, 2023. https://doi.org/10.1007/978-3-031-38857-6_27

additional advantage of *Drosophila* over other model organisms is that extensive work has been done in recent years to create a full connectome of their brains [26, 36], and the visual system in particular has been extensively studied [28,29,33].

The motion vision pathway is extremely important for adaptive behavior in Drosophila, aiding in estimation of body motion and enabling rapid response to oncoming threats [1,9,12]. The structure is well documented, see Fig. 1 for a visual representation and refer to [6] for a more thorough review. Within the Drosophila optic lobe, retinal and lamina cells convert changes in light intensity into information used in the rest of the network. Of particular relevance to the motion vision system are cells L1-L3, which perform spatiotemporal filtering of input stimuli and separate information flow into two pathways: an On pathway for encoding increases in brightness, and an Off pathway for encoding decreases in brightness [28,33]. From there, the transformed visual information is further filtered in the medulla into a bank of unique filters (Mi1, Tm3, Mi4, Mi9 for the On pathway; Tm1, Tm2, Tm4, Tm9 for the Off pathway), each with slightly different spatiotemporal characteristics [2,11]. These are then combined nonlinearly (along with the wide amacrine cell CT1 [24]) onto the elementary motion detector (EMD) cells T4 and T5, and the resulting combination generates directional selectivity for each point in the visual field [29] which can then be spatially integrated for more complex behavior [6].

Previous work has adapted this circuitry to robotics [4] and SNS networks [27], but these studies were performed before the wide breadth and depth of connectivity information from connectomic analysis for *Drosophila* became available. In this work, we design an SNS network which measures optic flow for both rising and falling brightness levels, using inspiration from the current body of knowledge about connectivity and activity within the *Drosophila* optic lobe [6,29]. As there is less known about the exact operation of the Off EMD, we make some design-based decisions in its construction. Using the capabilities of this network, we plan future visual control of motion onboard the bio-inspired robot *Drosophibot* [13].

2 Network Components

2.1 Neural and Synaptic Models

As this work is primarily focused on designing general network behavior instead of exactly reproducing neural recordings, all neurons in the network are simulated as non-spiking leaky integrators following [31], where the neural state U is updated as

$$\tau \cdot \dot{U} = -U + S + B + I,\tag{1}$$

where τ is the neural time constant, I is any external input, and B is a constant bias term. S is the synaptic input from any presynaptic neurons in the network,

$$S = \sum_{n=0}^{N} G_{syn,n} (U_n) \cdot (E_{syn,n} - U), \qquad (2)$$

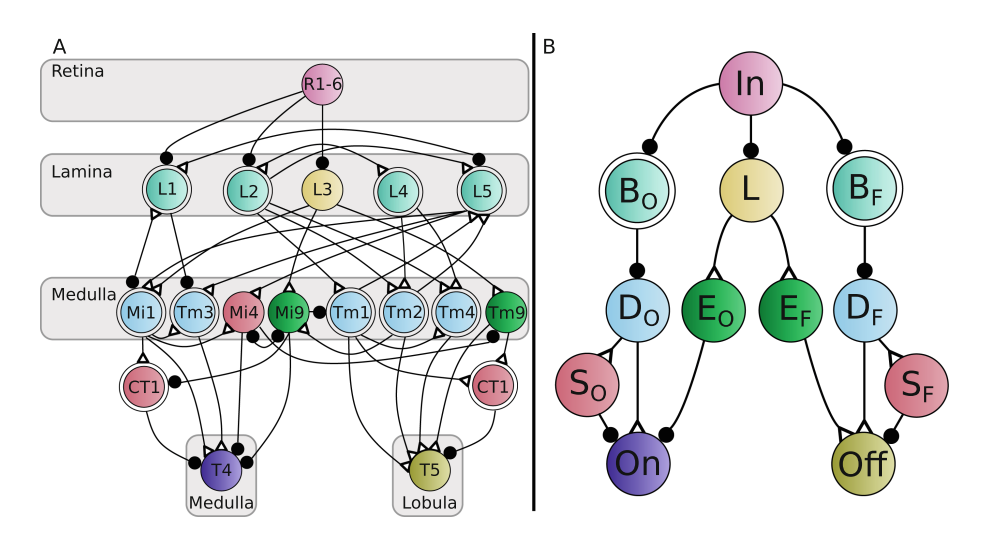


Fig. 1. A: A circuit diagram of a single column within the *Drosophila* motion vision pathway, adapted from [6,29]. **B:** Reduced diagram used in this work. Node colors in both diagrams are chosen to highlight their common functional roles. Single circles designate neurons which behave as a low-pass filter, double circles indicate a bandpass filter. Dark closed circles indicate inhibitory synapses, open triangles indicate excitatory synapses. In panel **B**, D and S neurons approximate band-pass behavior by filtering the responses of the B neurons, for reduced computational complexity.

with U_n denoting a presynaptic neuron, and $E_{syn,n}$ denoting the synaptic reversal potential. In this work, all excitatory synapses have $E_{ex} = 5R$, $E_{in} = -2R$ for inhibitory synapses, and specific modulatory synapses have a reversal potential of $E_{mod} = -0.1R$, where R is the primary range of neural activity in the network. For numerical simplicity, R = 1 in this work so that most neurons communicate when their state is between 0 and 1, with the exception of the synapse between neurons B_F and D_F . E_{ex} has an effect roughly analogous to cholinergic synapses in Drosophila, E_{in} to GABAergic synapses, and E_{mod} to glutamatergic synapses. $G_{syn,n}(U_n)$ is a monotonic function which describes the incoming synaptic conductance such that $G_{syn,n}(U_n) \in [0, g_{max,n}]$ where $g_{max,n}$ is the upper bound. In this work, we define G_{syn} as

$$G_{syn,n} = g_{max,n} \cdot max \left(0, min \left(\frac{U_n - \theta_{lo}}{\theta_{hi} - \theta_{lo}}, 1 \right) \right), \tag{3}$$

where θ_{lo} and θ_{hi} are the lower and upper threshold states of synaptic activity. For most synapses in the network, we set $\theta_{lo} = 0$, and $\theta_{hi} = R$. For the synapse between neurons B_F and D_F , we set $\theta_{lo} = R$, and $\theta_{hi} = 2R$.

Steady State Formulation. For some design sections, we required solving for the steady state of the neuron given steady inputs. As in [31], the steady-state response U^* is

$$U^* = \frac{\sum_{n=1}^{N} g_{max,n} \frac{U_n^*}{R} \cdot E_{syn,n} + B + I}{1 + \sum_{n=1}^{N} g_{max,n} \frac{U_n^*}{R}}.$$
 (4)

Synaptic Pathway Designs. When connecting components of our network, different pathways are tuned analytically based on their functional role. One common example is signal transmission, where the desired steady-state value (see Eq. 4) of the postsynaptic neuron U^* is the steady-state voltage of the presynaptic neuron multiplied by a transmission gain K. From [31], this can be solved as

$$g_{max} = \frac{K \cdot R}{E_{sym} - K \cdot R},\tag{5}$$

where E_{syn} is E_{ex} for excitatory synapses, and E_{in} for inhibitory synapses.

Another formulation which is used throughout this work comes from setting a target state T of the postsynaptic neuron, given a presynaptic steady-state and the presence of other external or synaptic currents to the postsynaptic neuron. This is derived from Eq. 4 and written as

$$g_{max} = \frac{R \cdot (B - T)}{U_{pre}^* \cdot (T - E_{syn})}.$$
 (6)

Finally, in some instances it is desirable for a presynaptic neuron to modulate the sensitivity of a postsynaptic neuron to external and synaptic inputs. For this we follow the derivation in [31], and use the modulatory reversal potential E_{mod} and set the synaptic conductance as

$$g_{max} = \delta - 1, (7)$$

where the desired behavior is such that U^* is divided by δ when $U^*_{pre} = R$. This form of synapse is used within the On pathway between E_O and On.

2.2 Neural Filters

Most neurons within the *Drosophila* motion vision pathway behave temporally as either low or band-pass filters [6], and here we describe our methodology in designing our network to behave accordingly. The process to tune our neurons as low-pass filters is straightforward, as the leaky integrator is itself a low-pass filter with a cutoff frequency (where the gain is -3dB) defined as $f_c = \frac{1}{2\pi\tau}$.

Common methods for implementing a neuron with band-pass temporal behavior typically involve adding a second dynamic variable to the neuron model [19], such as a voltage-gated ion channel [30] or adaptive spiking threshold [32,34]. Inspired by the differentiation network in [31], we implement bandpass filters in our network using a subnetwork of four non-spiking leaky integrators instead of adding a new, more complex neural model. While this adds more neurons to the network, we do this to reduce the computational complexity of our system in anticipation of running it on embedded hardware. For a visual representation, please see Fig. 2.

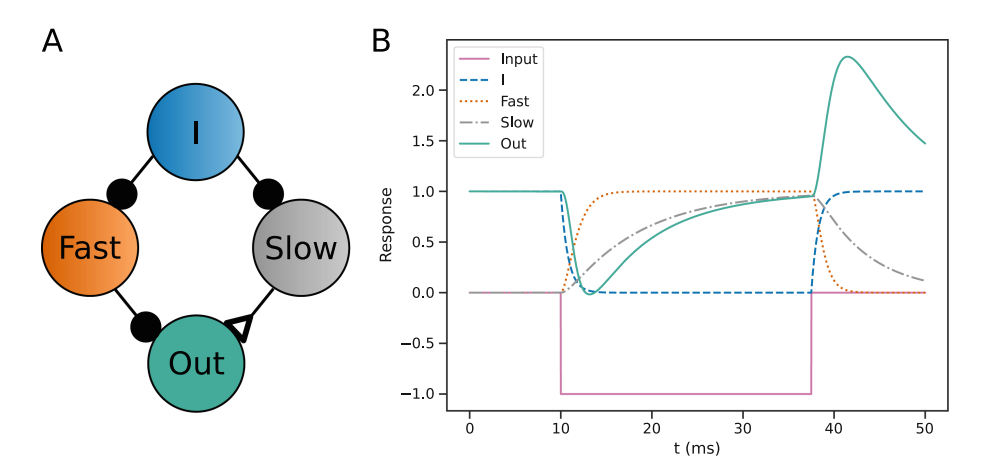


Fig. 2. A: Circuit diagram of a band-pass subnetwork. Two neurons are tuned as low-pass filters with different cutoff frequencies, and are subtracted to produce a band-pass response. **B:** Response of each neuron within the subnetwork when subjected to a time-varying input.

This network is designed as follows. Inputs to the subnetwork enter as a synaptic input for neuron I, which then inhibits neurons Fast and Slow using inhibitory transmission synapses (Eq. 5) with reversal potential E_{in} and a gain K = -1, to arrive at a maximum synaptic conductance of

$$g_{max,i,fast} = g_{max,i,slow} = -\frac{R}{E_{in}}. (8)$$

Neurons I, Slow, and output neuron Out all have the same time constant, which approximately acts as the upper bound of the filter's passband. Neuron Fast has a larger time constant and lower cutoff frequency than the other neurons, and the corresponding cutoff frequency results in setting the lower bound of the passband. Neuron Fast inhibits neuron Out with a gain-controlled inhibitory synapse (Eq. 5), and neuron Slow excites Out with a synapse designed to mirror $g_{max,fast,out}$, where

$$g_{max,slow,out} = \frac{g_{max,fast,out} \cdot (E_{in} - R)}{R - E_{ex}}.$$
 (9)

This results in the state of neuron Out being the difference between the original signal in I being processed via two different low-pass filters, resulting in a bandpass effect. In practice, the value of the transmission gain K from Fast to Out is found using the Brent method for scalar minimization [7] in SciPy [35] such that the change in magnitude during a step input is -1. All neurons in this subnetwork additionally have a constant bias input of R, since the bandpass filters in our network need to hyperpolarize during rising luminance levels, but omitting these bias terms and swapping the inhibitory and excitatory synapses would result in a more traditional band-pass filter [31].

3 Network Design

For a circuit diagram of the network described in this section, as well as the comparative structure present in the *Drosophila* optic lobe, please refer to Fig. 1. All synaptic parameter values can be found in Table 1, and all neural parameter values can be found in Table 2.

3.1 Input Processing

When presented with a visual stimulus, each input node (denoted In in Fig. 1B) acts as a temporal low-pass filter, performing an analogous operation to a Drosophila photoreceptor cell [8]. As this initial stage sets an upper bound on the frequency response for the rest of the circuit, we set the time constant for this filter τ_{fast} such that no frequencies in our desired input range are filtered out and our network dynamics remain stable. In this work, we set this as $\tau_{fast} = 10 \cdot \Delta t$ based on our simulation timestep Δt .

3.2 Initial Filter Stage

Similar to the cells present in the Drosophila lamina, we apply temporal filters to the output of the initial input filtering stage. While the primary lamina cells in the Drosophila motion pathway have slight differences in temporal behavior [11], for analytic simplicity both B_O and B_F have the same properties in this work. For reduced analytic complexity, all spatial receptive fields are condensed into single columns.

We apply a band-pass filter which hyperpolarizes to stimuli of increasing brightness within each pathway to the output of the input stage, analogous to the behavior of the L1 and L2 cells [6], and we refer to them as B_O and B_F . These are constructed in the manner described in Sect. 2.2, and the time constant of the fast side is set to τ_{fast} . For the slow side, we choose τ_{slow} so that for the fastest input stimulus, the response has time to settle to baseline over the course of a single input period. Approximating the settling period for a leaky integrator as 5τ , we write the time constraint as

$$5\tau_{slow} = \frac{\lambda}{2} \cdot \frac{1}{V_{fast}},\tag{10}$$

where λ is the spatial wavelength and V_{fast} is the fastest spatial velocity of the input stimulus.

Similar to the L3 neuron in Drosophila [6], we include an additional lowpass filter (denoted as L in Fig. 1B) which is shared across both the On and Off pathways. In order to preserve the range of temporal information available for later processing, we set the time constant of L to τ_{fast} , causing this node to act as a delayed and inverted copy of the input stimulus.

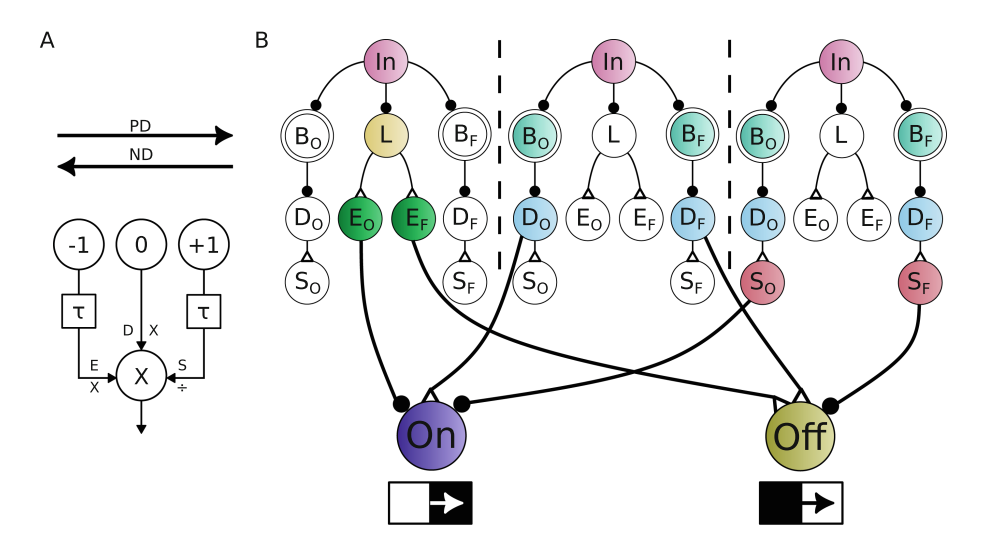


Fig. 3. A: Diagram of a three-arm Haag-Borst HR/BL EMD circuit [15]. B: Schematic of the three-arm motion detectors in this work, for both On and Off stimuli. PD denotes the preferred direction, ND denotes the not preferred (null) direction. Nodes without color do not contribute to behavior in this direction of motion.

3.3 Motion Detectors

For the design of the elementary motion detectors (EMD) in the On and Off pathways, we take inspiration from the Haag-Borst HR/BL three-arm EMD [15] (Fig. 3A). This structure has been shown to be capable of reproducing recordings from T4 [15] and T5 [16] cells, and connectomic analysis has found candidate cells for each input arm of the model [29]. In this model, the output neuron of each EMD (On for the On pathway, Off for the off pathway) receives input from three separate elements: a direct input from the cell in the same column, an enhancement input which enhances stimuli coming from the preferred direction, and a suppressor input which suppresses stimuli coming from the null direction. In this work we choose to model the EMD as a three-arm circuit instead of older models which used two arms to achieve either preferred-direction enhancement [17] or null-direction suppression [5], as the three-arm model generates finer directional selectivity and is less susceptible to noise [15].

In *Drosophila* the inputs in each arm can come from multiple neurons, which combine to create varied spatio-temporal properties [2,6,11]. For simplified analysis and reduced computational complexity, each arm is represented as a single neuron in this work. Additionally, while the cells in the medulla act as band-pass and low-pass filters with a variety of time constants, for simplicity we represent all of them as low-pass filters and reshape the activity from the higher-level filters (B_O , B_F , and L). In this work, neurons which perform enhancement are named E, direct stimulation D, and suppression S. Unless otherwise specified,

all neurons can be assumed to have a time constant of τ_{fast} . This is only changed as needed for behavioral reasons, which will be explained below.

On Pathway. Recent studies have focused on the behavior of T4 cells and found potential mechanisms which generate motion-detection and direction selectivity using the cells which contribute to the On pathway [29], particularly in the work of Groschner et al. [14]. In their work, they modeled the T4 pathway and found that multiplicative behavior can occur during a period of low inhibition that creates a "window of opportunity" [10]. We adapt a similar mechanism here based on our previous work [31], with a circuit diagram in Fig. 3B and behavior shown in Fig. 4. Neuron D_O mimics the behavior of Mi1 and Tm3, S_O the response of CT1, and E_O is analogous to Mi9.

Direct: Neuron D_O receives input from B_O via an inhibitory transmission synapse (Eq. 5), and the gain is tuned via Brent's method [7] such that the peak during a step input is 1. It excites On with an excitatory transmission synapse, with the gain tuned again via Brent's method for an isolated peak response of 1.

Suppression: Unlike the other arms of the On EMD, S_O receives input from D_O instead of the filtering stage. This is similar to CT1 receiving indirect input from Mi1 [24,29]. This creates a slight delay in the response, which improves the ability of S_O to suppress stimuli in the null direction. The connection between S_O and On is tuned as an inhibitory target synapse (Eq. 6) which aims to bring the state of On to zero when D_O is signaling with peak strength.

Enhancement: In our model, E_O is responsible for the majority of the stimulus-dependent behavior of the On EMD. Starting with the temporal response, we set the neural time constant so that the state of E_O settles during the time it takes the signal to travel from one column to the next at the slowest desired velocity V_{slow} , assuming that the neuron settles after a time period of 5τ (Eq. 10). This is found with

$$\tau_E = \frac{\angle}{5 \cdot V_{slow}},\tag{11}$$

where \angle is the spatial resolution of the model (5° in this work). E_O stimulates On using a modulatory synapse with a division factor δ of 10 (Eq. 7), and is stimulated by L using an excitatory transmission synapse (Eq. 5) with unity gain.

Off Pathway. While studies have found the presynaptic neurons which generate direction selectivity within the Off motion detector circuit [24,29], current studies which model the Off pathway either omit the role of CT1 in suppression [20] or do not model chemical reversal potentials [21]. As such, we make some base assumptions based on the connectivity in order to produce direction selectivity. Neuron D_F implements the role of Tm1, Tm2, and Tm4, S_F is analogous to CT1, and E_F mimics Tm9.

Direct: D_F receives stimulation from B_F via an excitatory transmission synapse (Eq. 5) with a gain tuned such that the postsynaptic peak is 1 for a decreasing step response in brightness, and θ_{lo} and θ_{hi} of R and 2R respectively. It stimulates Off with an excitatory target synapse of target R (Eq. 6), with the conductance multiplied by ρ_D , where ρ_D is the percentage of direct stimulation. In this work, $\rho_D = 0.5$. We found that the peak of D_F is a primary factor in the magnitude of Off, so we select the time constant τ_{DF} so that the peak magnitude starts decreasing at our slowest input velocity V_{slow} . We first find the frequency of our slowest input as $f_{slow} = \frac{V_{slow}}{\lambda}$, and scale that to get $f_{DF} = 10 f_{slow}$. A scaling factor of 10 is chosen because the gain of leaky integrators begins to decrease approximately 1 decade below the cutoff frequency on a logarithmic scale.

Suppression: S_F is tuned in a similar manner to S_O , receiving an excitatory transmission (Eq. 5) input from D_F that is optimized using Brent's method [7] for a peak magnitude of 1. S_F inhibits Off via an inhibitory target synapse with the same properties as the synapse between S_O and On.

Enhancement: E_F is tuned with the exact input and neural properties of E_O for simplicity. It stimulates Off with an excitatory target synapse (Eq. 6) with target R, and the conductance scaled by ρ_E where ρ_E is the percentage of enhancement stimulation and is constrained so $\rho_E + \rho_D = 1$.

4 Results

4.1 Simulation Setup

All simulations are done using SNS-Toolbox [25], a Python package for designing and simulating synthetic nervous systems (https://github.com/wnourse05/SNS-Toolbox). A Δt of 0.1 ms is used as the simulation step. In all simulations, the network was tuned for sensitivity to images with a spatial wavelength λ of 30° and a velocity between 10°/s and 180°/s across the visual field. Code to simulate the network and generate all of the figures presented here is available at https://github.com/wnourse05/Motion-Vision-SNS.

4.2 Individual EMD Stimulation

To verify the basic behavior of the EMD circuits, we applied square wave gratings with a spatial wavelength of 30° and a velocity of $30^{\circ}/s$ to 3 adjacent columns. We focus on the behavior of the B channel neurons, which are tuned for sensitivity in motion traveling from left to right.

Shown in Fig. 4, we examine the behavior of the On pathway. When stimuli of increasing brightness move across in the preferred direction, E_O receives the stimulus change first and starts to hyperpolarize. In the time it takes for the stimulus to continue to the central column, E_O has decreased. This allows the

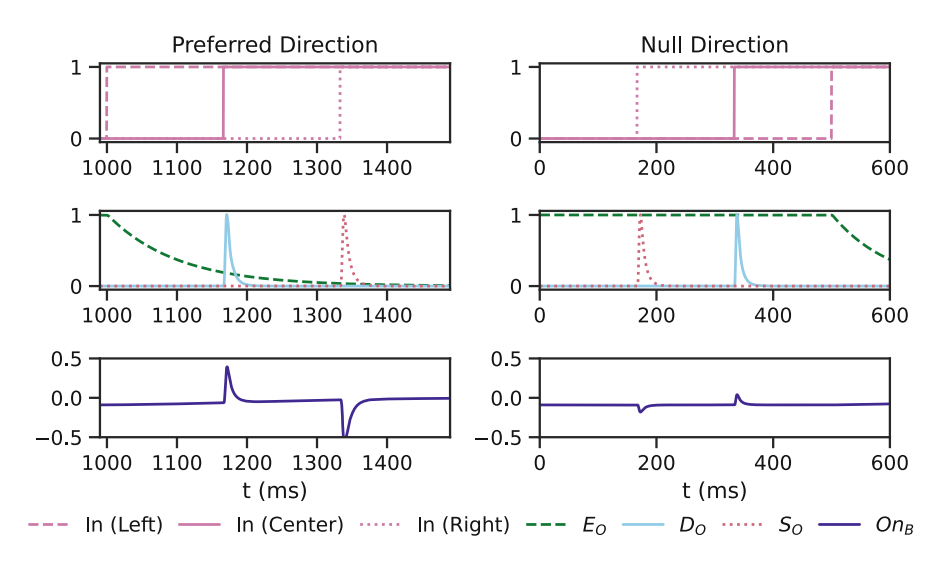


Fig. 4. Simulation of elements within the On pathway during a stimulus moving in the preferred (Left) or null (Right) directions. Dashed green traces correspond to Enhancement (E_O) signals, solid blue to Direct (D_O) signals, dotted pink to Suppression (S_O) signals, and solid indigo for the On EMD (On_B). Top: Traces of visual stimuli to the Enhancement, Direct, and Suppression columns of the motion detector; Middle: Traces of the Enhancement, Direct, and Suppression neurons which are presynaptic to the EMD neuron; Bottom: Trace of the final motion detector, which depolarizes for stimuli traveling from left to right (On_B).

direct stimulus from D_O to excite On with reduced inhibition. As the stimulus continues to the right column, S_O exhibits a bout of further inhibition. The timing relationship between E_O and S_O creates the speed-dependent behavior; as stimuli move more rapidly, the offset in time between these columns decreases and more inhibition is applied to On, causing a decrease in the activity caused by D_O . When stimuli move in the opposite direction, S_O and D_O are both activated while E_O is strongly depolarized, resulting in a significant reduction of peak magnitude in On.

Repeating the experiment for stimuli with decreasing brightness, as the offedge stimulus moves in the preferred direction E_F in the Off pathway begins to depolarize. This is accentuated by a later pulse from D_F , followed by strong inhibition from S_F . As stimuli move in the opposite direction, E_F is either at rest or hyperpolarizing towards rest, depending on the timing of prior stimuli. The off-edge first arrives at S_F which strongly inhibits Off, followed by a pulse in excitation from D_F and then a separate increase in excitation from E_F . While the specifics of the mechanism are different between the On and Off pathways, the net behavioral result is the same: stimuli traveling in the preferred direction are enhanced to some degree, while stimuli in the opposite direction do not have as strong a response (Fig. 5).

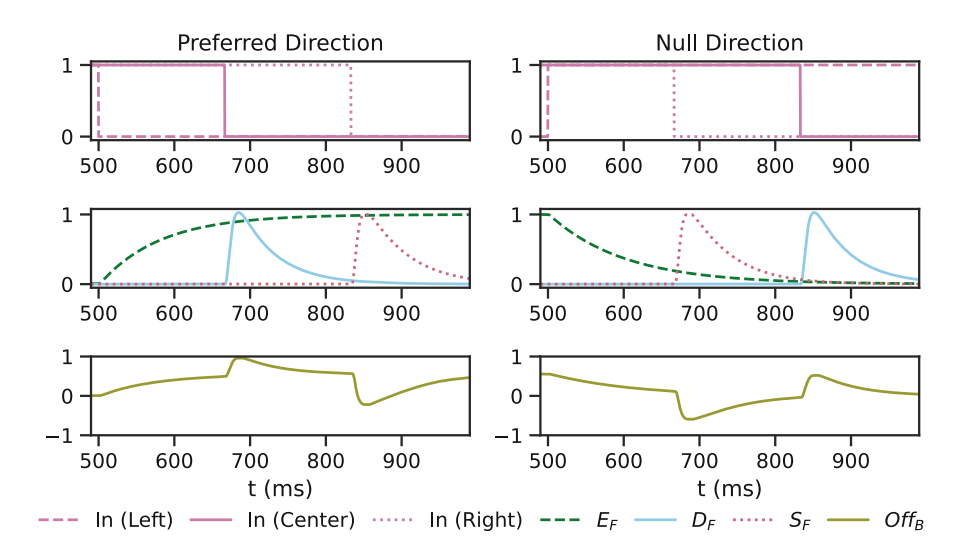


Fig. 5. Simulation of elements within the Off pathway during a stimulus moving in the preferred (Left) or null (Right) directions. Dashed green traces correspond to Enhancement (E_F) signals, solid blue to Direct (D_F) signals, dotted pink to Suppression (S_F) signals, and solid olive for the Off EMD (Off_B). For further description refer to Fig. 4.

4.3 Velocity Response

Square-wave stimuli with $\lambda=30^\circ$ are applied to a network which consisted of 49 columns, arranged in a 7×7 grid. The velocity of stimuli is varied from $10^\circ/s$ to $360^\circ/s$, and data is recorded from the central EMD. As shown in Fig. 6, the peak magnitude of both the On and Off pathways decreases as the velocity approaches the maximum tuning range $(180^\circ/s)$. The On pathway has a high dynamic range, varying smoothly from 1 to near zero, and with peaks in the preferred direction always greater than the null direction. Changes in the magnitude of the Off pathway are more gradual as it approaches the desired maximum velocity, with a slow increase slightly before this point. The ratio between the preferred and null directions is always greater than 1, but to a lesser degree in the Off than the On pathway. Behavior in the *Drosophila* T4 and T5 cells are more similar to the On results shown in Fig. 6 than the Off results, with a peak response that decreases as the input velocity increases [23]. However, in *Drosophila* this decrease occurs as input velocity is both increased and decreased from a peak velocity.

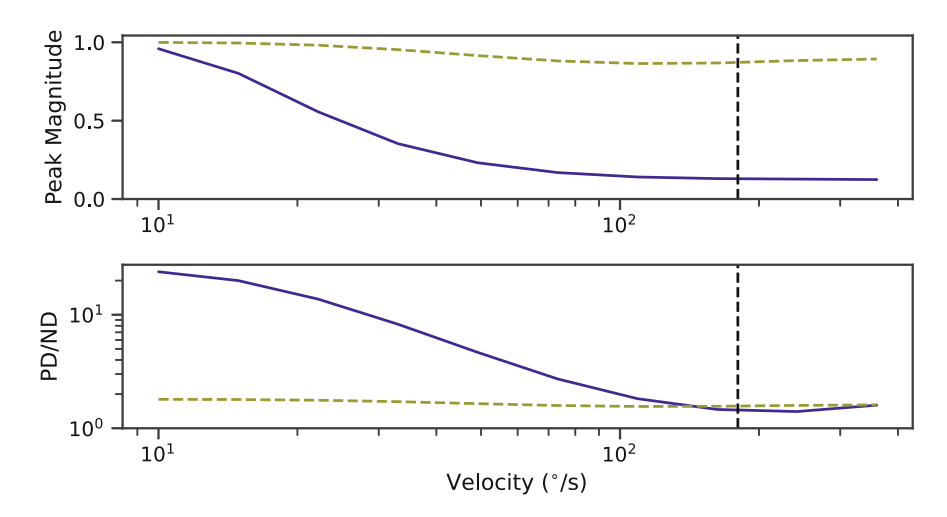


Fig. 6. Output behavior of the On (solid indigo) and Off (dashed olive) motion detectors when subjected to a square wave, translating from 10° to 360° per second. Target maximum velocity ($180^{\circ}/s$) shown with a vertical dashed line. *Top:* Peak magnitude of the motion detector in the preferred direction; *Bottom:* Ratio between the motion detector in the preferred direction and the null direction.

4.4 Directional Selectivity

Stimuli of a consistent wavelength and velocity are applied to the same network described in Sect. 4.3 while the direction of travel is varied from $0^{\circ} - 360^{\circ}$ in 45° increments, with results shown in Fig. 7. The EMD for each cardinal direction exhibits enhanced sensitivity to stimuli in the preferred direction, and reduced sensitivity to the other directions. The On pathway is able to generate a finer level of directional sensitivity than the Off pathway, due to its multiplicative window of reduced inhibition. Further work is necessary to find a similar multiplication mechanism for the Off pathway.

As the networks for each cardinal direction are mirrored versions of each other, the resulting responses are identical except for their orientation. This is different than the tuning found in Drosophila, where the sensitivity of each cardinal direction is slightly different [23]. The general shape of our On and Off responses most closely matches the behavior of the T4b and T5b neurons in the animal, consisting of a sharp triangular point in the preferred direction and a slight bump in the null direction, however T5b is much more similar to T4b than our Off neurons are to the On neurons.

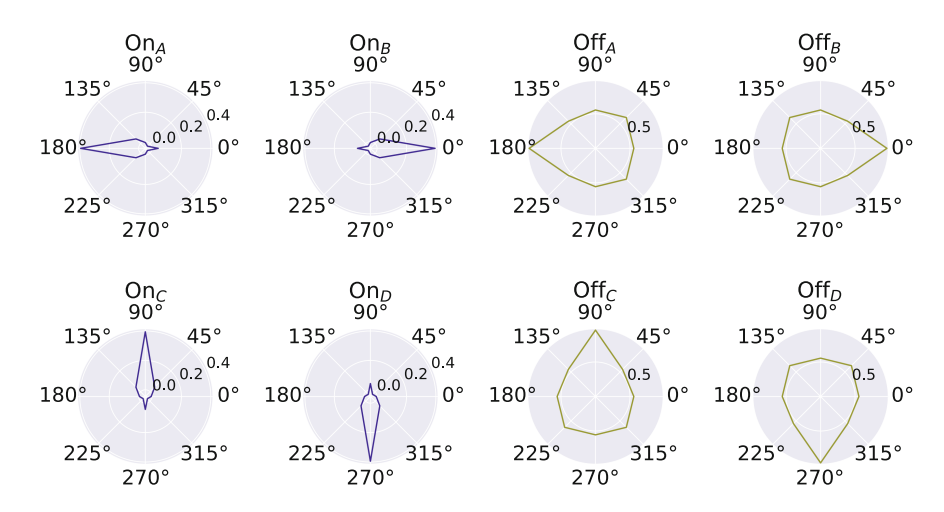


Fig. 7. Peak response of each motion detector in the On (*Left*) and Off (*Right*) pathways to a square wave grating with $\lambda = 30^{\circ}$ and $V = 30^{\circ}/s$. Preferred direction of each sub-type: A: right to left; B: left to right C: bottom to top; D: top to bottom.

5 Discussion and Future Work

In this work, we implement an SNS network which is a reduced model of the *Drosophila* motion vision system. The network performs optic flow measurement at each point in the visual field, and can be tuned for different ranges of input stimuli in a parametric manner. While some parameters are found via numerical optimization, most are chosen by hand via analytic rules. With further optimization, we expect that the performance of the network could be tuned to detect particular stimuli.

Compared to the circuit found in Drosophila, the model presented here is far reduced in complexity. In particular, the animal uses more neurons as inputs to the EMD cells, which allows for better temporal response and additional adaptation to factors such as changing input contrast [11]. Adding more neurons into the motion detection area in our network may be promising for future development. Another simplification in our model is that the initial filter stage only receives visual input within its own column. This is not the case for the lamina neurons in Drosophila, which perform spatial filtering over a $15^{\circ} - 20^{\circ}$ radius for each column [6]. Future work will extend our analysis to generate directional selectivity in the presence of wider spatial receptive fields.

While our implementation of the On pathway is derived from detailed biological models [14], less recordings and detail were available for the Off pathway. Our model attempts to model direction selectivity using current information about the structure of this system, but showcases some current gaps in understanding. In particular, the neuron in our model which is intended to act analogously to

Tm9 (E_F) does not provide a significant role in motion detection based on its connectivity. This differs strongly from biological experiments, where the effect of Tm9 in Off motion detection is greater than many of the other neurons combined [28]. As such Tm9 may have additional functionality and roles, as discussed in [29].

Much work has been done to study the effect of the visual system on walking control in Drosophila [9,12]. We aim to continue development of the network described in this work, so that it may be used to assist in the control of legged motion onboard our Drosophila-inspired robot, Drosophilot [13].

~			_	_
Synapse	g_{max}	E_{syn}	θ_{lo}	θ_{hi}
$In \rightarrow B_{O,I}$	0.5	-2.0	0.0	1.0
$In \rightarrow B_{F,I}$	0.5	-2.0	0.0	1.0
$In \rightarrow L$	0.5	-2.0	0.0	1.0
$B_{O,I} \rightarrow B_{O,Fast}$	0.5	-2.0	0.0	1.0
$B_{O,I} \to B_{O,Slow}$	0.5	-2.0	0.0	1.0
$B_{O,Fast} \rightarrow B_{O,Out}$	1.329*	-2.0	0.0	1.0
$B_{O,Slow} \rightarrow B_{O,Out}$	0.997	5.0	0.0	1.0
$B_{F,I} o B_{F,Fast}$	0.5	-2.0	0.0	1.0
$B_{F,I} o B_{F,Slow}$	0.5	-2.0	0.0	1.0
$B_{F,Fast} \rightarrow B_{F,Out}$	1.329*	-2.0	0.0	1.0
$B_{F,Slow} \rightarrow B_{F,Out}$	0.997	5.0	0.0	1.0
$L \to E_O$	0.25	5.0	0.0	1.0
$L \to E_F$	0.25	5.0	0.0	1.0
$B_{O,Out} \to D_O$	0.546^{*}	-2.0	0.0	1.0
$B_{F,Out} \to D_F$	1.173*	5.0	1.0	2.0
$D_O \to S_O$	0.262^{*}	5.0	0.0	1.0
$D_F \to S_F$	0.250^{*}	5.0	0.0	1.0
$E_O \to On$	9.0	-0.1	0.0	1.0
$D_O \to On$	0.262*	5.0	0.0	1.0
$S_O \to On$	0.5	-2.0	0.0	1.0
$E_F \to Off$	0.125	5.0	0.0	1.0
$D_F o Off$	0.125	5.0	0.0	1.0
$S_F \to Off$	0.5	-2.0	0.0	1.0

^{*}Found using optimization

Name	$\tau \text{ (ms)}$	В	U_0
In	1.0	0.0	0.0
$B_{O,In}$	0.796	1.0	1.0
$B_{O,Fast}$	1.0	1.0	0.0
$B_{O,Slow}$	8.334	1.0	0.0
$B_{O,Out}$	0.796	1.0	1.0
$B_{F,In}$	0.796	1.0	1.0
$B_{F,Fast}$	1.0	1.0	0.0
$B_{F,Slow}$	8.334	1.0	0.0
$B_{F,Out}$	0.796	1.0	1.0
\overline{L}	1.0	1.0	1.0
E_O	100.0	0.0	1.0
E_F	100.0	0.0	1.0
D_O	1.0	1.092*	0.0
D_F	47.746	0.0	0.0
S_O	1.0	0.0	0.0
$\overline{S_F}$	1.0	0.0	0.0
\overline{On}	1.0	0.0	0.0
L	1.0	0.0	0.0

Table 2. Neuron Parameter Values.

References

- Ache, J.M., et al.: Neural basis for looming size and velocity encoding in the Drosophila giant fiber escape pathway. Curr. Biol. 29, 1073–1081.e4 (2019). https://doi.org/10.1016/j.cub.2019.01.079
- Arenz, A., Drews, M.S., Richter, F.G., Ammer, G., Borst, A.: The temporal tuning of the Drosophila motion detectors is determined by the dynamics of their input elements. Curr. Biol. 27, 929–944 (2017). https://doi.org/10.1016/j.cub.2017.01. 051
- Ayers, J., Witting, J.: Biomimetic approaches to the control of underwater walking machines. Philos. Trans. R. Soc. A: Math. Phys. Eng. Sci. 365(1850), 273–295 (2007)
- Bagheri, Z.M., Wiederman, S.D., Cazzolato, B.S., Grainger, S., O'Carroll, D.C.: Performance of an insect-inspired target tracker in natural conditions. Bioinspiration Biomimetics 12 (2017). https://doi.org/10.1088/1748-3190/aa5b48
- Barlow, H., Levick, W.R.: The mechanism of directionally selective units in rabbit's retina. J. Physiol. 178(3), 477 (1965)
- Borst, A., Drews, M., Meier, M.: The neural network behind the eyes of a fly (2020). https://doi.org/10.1016/j.cophys.2020.05.004
- Brent, R.P.: Algorithms for Minimization Without Derivatives. Courier Corporation (2013)

^{*}Found using optimization

- Clark, D.A., Demb, J.B.: Parallel computations in insect and mammalian visual motion processing (2016). https://doi.org/10.1016/j.cub.2016.08.003
- Creamer, M.S., Mano, O., Clark, D.A.: Visual control of walking speed in Drosophila. Neuron 100, 1460–1473.e6 (2018). https://doi.org/10.1016/j.neuron. 2018.10.028
- Denève, S., Machens, C.K.: Efficient codes and balanced networks (2016). https://doi.org/10.1038/nn.4243
- 11. Drews, M.S., et al.: Dynamic signal compression for robust motion vision in flies. Curr. Biol. 30, 209–221.e8 (2020). https://doi.org/10.1016/j.cub.2019.10.035
- Fujiwara, T., Brotas, M., Chiappe, M.E.: Walking strides direct rapid and flexible recruitment of visual circuits for course control in Drosophila. Neuron 110, 2124– 2138.e8 (2022). https://doi.org/10.1016/j.neuron.2022.04.008
- 13. Goldsmith, C.A., Szczecinski, N.S., Quinn, R.D.: Neurodynamic modeling of the fruit fly Drosophila melanogaster. Bioinspiration Biomimetics 15, 065003 (2020)
- Groschner, L.N., Malis, J.G., Zuidinga, B., Borst, A.: A biophysical account of multiplication by a single neuron. Nature 603, 119–123 (2022). https://doi.org/ 10.1038/s41586-022-04428-3
- Haag, J., Arenz, A., Serbe, E., Gabbiani, F., Borst, A.: Complementary mechanisms create direction selectivity in the fly. eLife 5 (2016). https://doi.org/10.7554/eLife.17421.001
- Haag, J., Mishra, A., Borst, A.: A common directional tuning mechanism of Drosophila motion-sensing neurons in the on and in the off pathway (2017). https://doi.org/10.7554/eLife.29044.001
- 17. Hassenstein, B., Reichardt, W.: Systemtheoretische analyse der zeit-, reihenfolgenund vorzeichenauswertung bei der bewegungsperzeption des rüsselkäfers chlorophanus. Zeitschrift für Naturforschung B 11(9–10), 513–524 (1956)
- 18. Hunt, A., Szczecinski, N., Quinn, R.: Development and training of a neural controller for hind leg walking in a dog robot. Front. Neurorobot. 11 (2017)
- 19. Izhikevich, E.M.: Dynamical Systems in Neuroscience: The Geometry of Excitability and Burtsing (2007). https://doi.org/10.1017/S0143385704000173
- Kohn, J.R., Portes, J.P., Christenson, M.P., Abbott, L., Behnia, R.: Flexible filtering by neural inputs supports motion computation across states and stimuli. Curr. Biol. 31(23), 5249–5260 (2021)
- Lappalainen, J.K., et al.: Connectome-constrained deep mechanistic networks predict neural responses across the fly visual system at single-neuron resolution. bioRxiv, pp. 2023–03 (2023)
- Leuba, G., Kraftsik, R.: Changes in volume, surface estimate, three-dimensional shape and total number of neurons of the human primary visual cortex from midgestation until old age. Anat. Embryol. 190, 351–366 (1994)
- 23. Maisak, M.S., et al.: A directional tuning map of drosophila elementary motion detectors. Nature **500**(7461), 212–216 (2013)
- 24. Meier, M., Borst, A.: Extreme compartmentalization in a Drosophila amacrine cell. Curr. Biol. 29, 1545–1550.e2 (2019). https://doi.org/10.1016/j.cub.2019.03.070
- Nourse, W.R., Szczecinski, N.S., Quinn, R.D.: SNS-toolbox: A tool for efficient simulation of synthetic nervous systems. In: Hunt, A., et al. (eds.) Biomimetic and Biohybrid Systems. Living Machines 2022. LNAI, vol. 13548, pp. 32–43. Springer, Cham (2022). https://doi.org/10.1007/978-3-031-20470-8_4
- Scheffer, L.K., et al.: A connectome and analysis of the adult drosophila central brain. Elife 9, e57443 (2020)

- 27. Sedlackova, A., Szczecinski, N.S., Quinn, R.D.: A synthetic nervous system model of the insect optomotor response. In: Vouloutsi, V., et al. (eds.) Living Machines 2020. LNCS (LNAI), vol. 12413, pp. 312–324. Springer, Cham (2020). https://doi.org/10.1007/978-3-030-64313-3_30
- 28. Serbe, E., Meier, M., Leonhardt, A., Borst, A.: Comprehensive characterization of the major presynaptic elements to the Drosophila off motion detector. Neuron 89, 829–841 (2016). https://doi.org/10.1016/j.neuron.2016.01.006
- 29. Shinomiya, K., et al.: Comparisons between the on-and off-edge motion pathways in the *Drosophila* brain (2019). https://doi.org/10.7554/eLife.40025.001
- 30. Szczecinski, N.S., Hunt, A.J., Quinn, R.D.: Design process and tools for dynamic neuromechanical models and robot controllers. Biol. Cybern. 111, 105–127 (2017). https://doi.org/10.1007/s00422-017-0711-4
- 31. Szczecinski, N.S., Hunt, A.J., Quinn, R.D.: A functional subnetwork approach to designing synthetic nervous systems that control legged robot locomotion. Front. Neurorobot. 11 (2017)
- 32. Szczecinski, N.S., Quinn, R.D., Hunt, A.J.: Extending the functional subnetwork approach to a generalized linear integrate-and-fire neuron model. Front. Neurorobot. 14 (2020). https://doi.org/10.3389/fnbot.2020.577804
- Takemura, S.Y., Nern, A., Chklovskii, D.B., Scheffer, L.K., Rubin, G.M., Meinertzhagen, I.A.: The comprehensive connectome of a neural substrate for 'on' motion detection in Drosophila (2017). https://doi.org/10.7554/eLife.24394.001
- 34. Teeter, C., et al.: Generalized leaky integrate-and-fire models classify multiple neuron types. Nat. Commun. 9 (2018). https://doi.org/10.1038/s41467-017-02717-4
- 35. Virtanen, P., et al.: SciPy 1.0 contributors: SciPy 1.0: fundamental algorithms for scientific computing in Python. Nat. Methods 17, 261–272 (2020). https://doi.org/10.1038/s41592-019-0686-2
- 36. Winding, M., et al.: The connectome of an insect brain. Science (New York, N.Y.) 379, eadd9330 (2023). https://doi.org/10.1126/science.add9330
- 37. Yu, W., et al.: Visual-locomotion: learning to walk on complex terrains with vision